Ground Penetrating Radar: Datasets and Applications from SnowEx

Webb, R.W., D. McGrath, R. Bonnell, T. Meehan, H.P. Marshall

Background

- Ground Penetrating Radar (GPR) has been collected in all SnowEx field campaigns

Figure 1. GPR sled being towed by R. Webb during SnowEx 2017 on Grand Mesa, CO.

Figure 2. Radar mounted on HP Marshall's snowmobile during SnowEx 2023 in Alaska.

Figure 3. GPR mounted on T. Meehan's snowmobile during SnowEx 2023 in Alaska.

Figure 4. GPR sled being pulled by R. Bonnell during SnowEx 2020 at Cameron Pass, CO.

Why GPR?

1. GPR signal is sensitive to snow density
   a. Snow Density has been shown to vary at scales difficult to observe by pits with standard surveys.
2. Provides near-continuous data over multiple km of transects

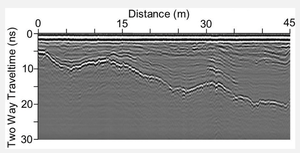

Figure 5. Example radargram with the strong reflection from the ground shown.

3. When combined with other methods, GPR provides density distribution data product.
4. Excellent SWE & density datasets for evaluating airborne (UAVSAR, SWESARR, etc.) and/or spaceborne products (Sentinel-1, NISAR, etc.)
5. GPR can be more accurate than traditional depth-based methods for estimating SWE.

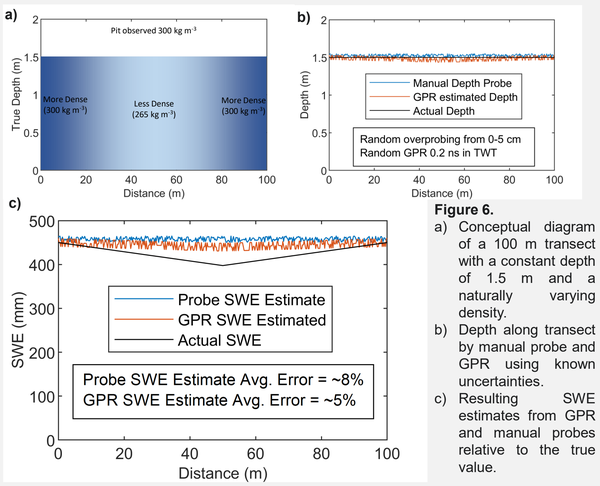

Figure 6.
a) Conceptual diagram of a 100 m transect with a constant depth of 1.5 m and a naturally varying density.
b) Depth along transect by manual probe and GPR using known uncertainties.
c) Resulting SWE estimates from GPR and manual probes relative to the true value.

Applications as Demonstrated in Publications

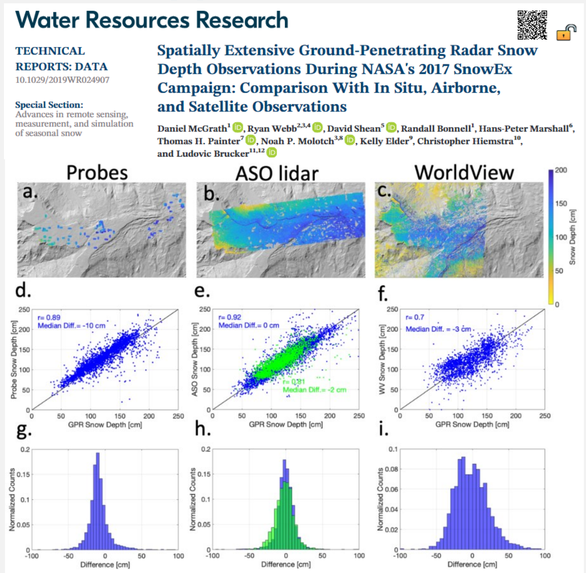

Figure 4. Snow depth derived from a manual probes, b ASO lidar DTMs, and c WorldView satellite DSMs. Scatterplots of snow depth from d manual probes, e ASO lidar DTMs, and f WorldView satellite DSMs compared to GPR-derived snow depths. Blue points in (e) and (f) have ASO-derived canopy heights <2 m, and green points have ASO-derived canopy heights >2 m. histograms of difference between (g) GPR-probes, (h) GPR-ASO, and (i) GPR-WorldView.

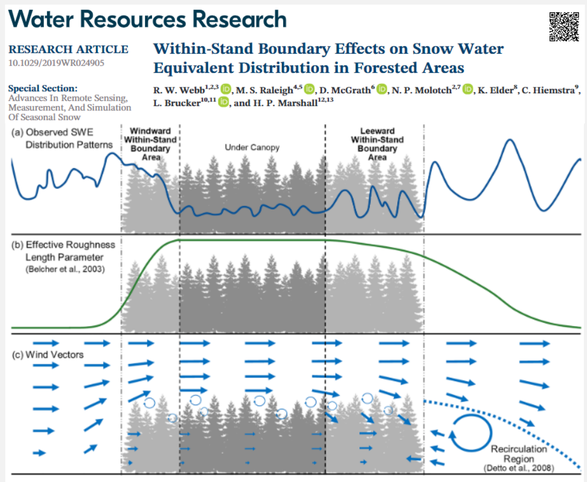

Figure 9. Conceptual diagram of the wind dynamics that occur around a forest stand in the direction of wind. Shown here is (a) representative pattern of snow water equivalent (SWE) distribution observed in this study using relative depths of Transect 56 for the windward edge and boundary effect and Transect 3 for the middle section, leeward boundary effect, and leeward edge, (b) the relative effective roughness length parameter when adjusted for fetch along the distance of a forest stand (Belcher et al., 2003), and (c) wind vectors that are expected as a result of the effective roughness length parameter and recirculation region on the leeward edge of the stand (Detto et al., 2008).

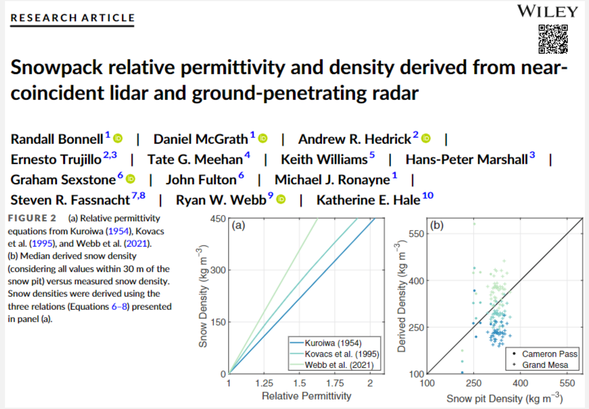

FIGURE 2 (a) Relative permittivity equations from Kuroiwa (1954), Kovacs et al. (1995), and Webb et al. (2021). (b) Median derived snow density (considering all values within 30 m of the snow pit) versus measured snow density. Snow densities were derived using the three relations (Equations 6–8) presented in panel (a).

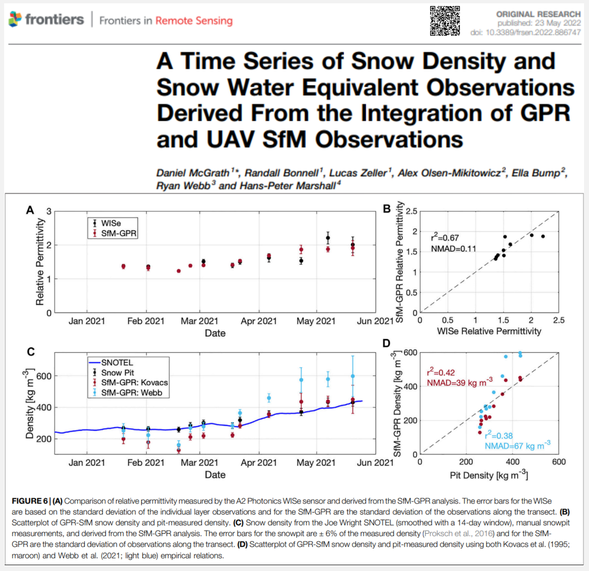

FIGURE 6 | (A) Comparison of relative permittivity measured by the A2 Photonics WISe sensor and derived from the SfM-GPR analysis. The error bars for the WISe are based on the standard deviation of the individual layer observations and for the SfM-GPR are the standard deviation of the observations along the transect. **(B)** Scatterplot of GPR-SfM snow density and pit-measured density. **(C)** Snow density from the Joe Wright SNOTEL (smoothed with a 14-day window), manual snowpit measurements, and derived from the SfM-GPR analysis. The error bars for the snowpit are ± 6% of the measured density (Proksch et al., 2016) and for the SfM-GPR are the standard deviation of observations along the transect. **(D)** Scatterplot of GPR-SfM snow density and pit-measured density using both Kovacs et al. (1995; maroon) and Webb et al. (2021; light blue) empirical relations.

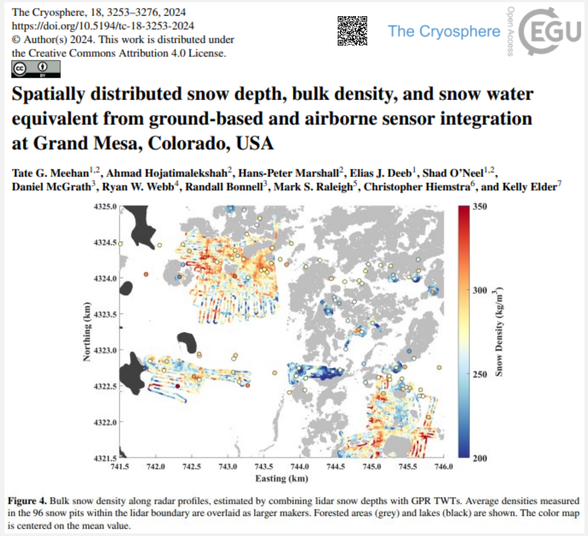

Figure 4. Bulk snow density along radar profiles, estimated by combining lidar snow depths with GPR TWTs. Average densities measured in the 96 snow pits within the lidar boundary are overlaid as larger makers. Forested areas (grey) and lakes (black) are shown. The color map is centered on the mean value.

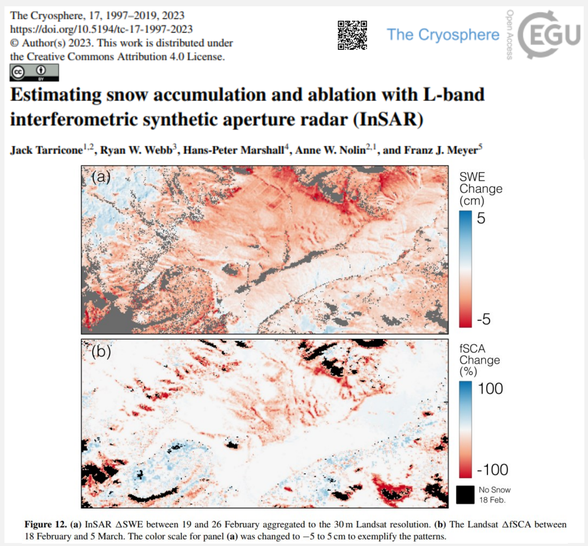

Figure 12. (a) InSAR ΔSWE between 19 and 26 February aggregated to the 30 m Landsat resolution. **(b)** The Landsat ΔfSCA between 18 February and 5 March. The color scale for panel **(a)** was changed to −5 to 5 cm to exemplify the patterns.

Paper in Review

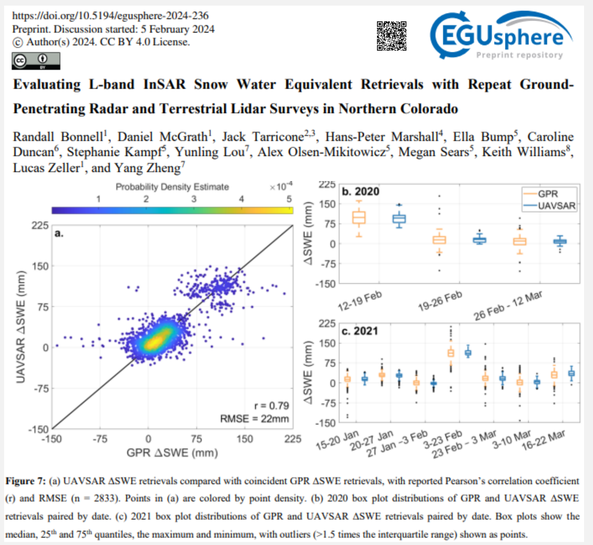

Figure 7: (a) UAVSAR ΔSWE retrievals compared with coincident GPR ΔSWE retrievals, with reported Pearson's correlation coefficient (*r*) and RMSE (n = 2833). Points in (a) are colored by point density. (b) 2020 box plot distributions of GPR and UAVSAR ΔSWE retrievals paired by date. (c) 2021 box plot distributions of GPR and UAVSAR ΔSWE retrievals paired by date. Box plots show the median, 25th and 75th quantiles, the maximum and minimum, with outliers (>1.5 times the interquartile range) shown as points.

Published Datasets

QR code to all SnowEx GPR data at NSIDC

SnowEx 2017:

Webb, R., McGrath, D., Hale, K. & Molotch, N. P. (2019). SnowEx17 Ground Penetrating Radar, Version 2 [Data Set]. Boulder, Colorado USA. NASA National Snow and Ice Data Center Distributed Active Archive Center. https://doi.org/10.5067/G21LGCNLFSC5.

SnowEx 2020:

Bonnell, R., McGrath, D., Webb, R. & Marshall, H. (2021). SnowEx20 Grand Mesa IOP CSU 1GHz GPR, Version 1 [Data Set]. Boulder, Colorado USA. NASA National Snow and Ice Data Center Distributed Active Archive Center. https://doi.org/10.5067/S5EGFLCIAB18.

McGrath, D., Bonnell, R., Olsen-Mikitowicz, A., Duncan, C. & Grabowski, J. (2021). SnowEx20 Cameron Pass Ground Penetrating Radar, Version 1 [Data Set]. Boulder, Colorado USA. NASA National Snow and Ice Data Center Distributed Active Archive Center. https://doi.org/10.5067/U4Q3X27BMRR4.

Meehan, T. G. (2021). SnowEx20 Grand Mesa IOP BSU 1 GHz Multi-polarization GPR CMP Snow Water Equivalent, Version 1 [Data Set]. Boulder, Colorado USA. NASA National Snow and Ice Data Center Distributed Active Archive Center. https://doi.org/10.5067/SOFEX3867ECJ.

Meehan, T. G. (2021). SnowEx20 Grand Mesa IOP BSU Multi-polarization 1 GHz GPR CMP Travel-Times, Version 1 [Data Set]. Boulder, Colorado USA. NASA National Snow and Ice Data Center Distributed Active Archive Center. https://doi.org/10.5067/SBFHOZ7F5WHS.

Webb, R. (2021). SnowEx20 Grand Mesa IOP UNM 800 and 1600 MHz MALA GPR, Version 1 [Data Set]. Boulder, Colorado USA. NASA National Snow and Ice Data Center Distributed Active Archive Center. https://doi.org/10.5067/WE9GI1GVMQF6.

Webb, R. (2021). SnowEx20 Jemez UNM 800 MHz MALA GPR, Version 1 [Data Set]. Boulder, Colorado USA. NASA National Snow and Ice Data Center Distributed Active Archive Center. https://doi.org/10.5067/H38Q5FTBPZ8K.

SnowEx 2021:

Bonnell, R., McGrath, D., Zeller, L., Bump, E. & Olsen-Mikitowicz, A. (2022). SnowEx21 Cameron Pass Ground Penetrating Radar, Version 1 [Data Set]. Boulder, Colorado USA. NASA National Snow and Ice Data Center Distributed Active Archive Center. https://doi.org/10.5067/SRWGLYCB6ZC4.

SnowEx 2023:

Webb, R. (2024). SnowEx23 University of Wyoming Ground Penetrating Radar, Version 1 [Data Set]. Boulder, Colorado USA. NASA National Snow and Ice Data Center Distributed Active Archive Center. https://doi.org/10.5067/H3D9IT1W6JT6.

Other GPR data from 2023 has been submitted and is in the process of being published.

Acknowledgements

This work was supported by the NASA Terrestrial Hydrology Program Awards: 80NSSC18K0877, 80NSSC18K1405, and NASA FINESST award 80NSSC20K1624

This work could not have been done without the great support of the larger SnowEx community and leadership group. The effort in planning prior to campaigns, ensuring quality data collection in a safe manner during campaigns, and curating data after campaigns takes an incredible amount of time. Thank you all! This work would not be possible without you.